IFAC Journal of Systems and Control 36 (2026) 100405

Contents lists available at ScienceDirect

IFAC Journal of Systems and Control

journal homepage: www.elsevier.com/locate/ifacsc

Full length article

Enhancing myoelectric control using a hybrid Frisch scheme and non-negative matrix factorization model for sEMG-based hand motion regression☆

Roberto Meattini *, Francesco Monti, Luca Bertozzi, Hamid Sohrabi, Davide Bargellini, Roberto Diversi

Dept. of Electrical, Electronic and Information Engineering (DEI) University of Bologna, Viale del Risorgimento 2, 40136 Bologna, Italy

ARTICLE INFO

Article history:
Received 2 November 2025
Received in revised form 19 February 2026
Accepted 3 March 2026
Available online 10 March 2026

Keywords:
Frisch scheme
Non-negative matrix factorization
Muscle synergies
Myoelectric control

ABSTRACT

Continuous myoelectric control of prosthetic and robotic hands requires robust regression of functional motion from surface electromyographic (sEMG) signals. However, sEMG recordings are affected by measurement noise, cross-talk, and overlapping muscle activity, which can degrade factorization-based decoding methods such as Non-Negative Matrix Factorization (NMF). We propose a hybrid approach that integrates the Frisch scheme, an Errors-in-Variables noise-consistent estimation method, with NMF-based muscle synergy extraction. The Frisch stage estimates noise-consistent linear relations among sEMG channels prior to factorization, improving the statistical structure of the data entering the NMF model. The resulting framework enables regression of continuous hand motion activation signals suitable for proportional control. Standard NMF, sparse NMF with multiplicative updates (NMF-MU), sparse NMF with alternating least squares (NMF-ALS), and the hybrid Frisch-based approach were evaluated on experimental data from five healthy subjects performing four functional hand gestures. Results show that the proposed Frisch+NMF approach achieves significantly lower reconstruction error compared to non-hybrid methods, demonstrating that noise-aware preprocessing enhances synergy-based myoelectric regression. The proposed methodology provides a principled and interpretable strategy for improving continuous sEMG-driven artificial hand control.

1. Introduction

Achieving human-like dexterity in robotic grasping remains one of the most challenging goals in robotics and neuroengineering, demanding precise, adaptable, and reliable interpretation of bioelectrical signals to classify hand postures for prosthetic or teleoperated control (Young et al., 2012). Although effective in controlled settings, discrete classification limits fluid, natural prosthetic control, motivating continuous sEMG-based mapping to multiple degrees of freedom (Jiang et al., 2008). However, several challenges are still present in continuous myoelectric control, especially related to the accuracy of multiple grasping intent detection. Typically, performance tends to deteriorate due to noise and non-idealities such as *cross-talk* among sEMG electrodes (De Luca et al., 2010) and nonstationarity of the biological signal, which lead to an overall degradation in the robustness of regression models used to reliably decode sEMG signals (Jiang et al., 2008; Rehbaum et al., 2012). These challenges highlight the need for representations that capture the coordinated structure underlying muscle activations rather than treating each channel independently. The concept of *synergies* provides a compelling neurophysiological rationale for addressing this complexity. Both postural synergies (Santello et al., 1998) and muscular synergies (Santello et al., 2016; Ting & McKay, 2007) propose that the central nervous system streamlines movement by combining a few coordinated activation patterns. Non-negative matrix factorization (NMF) (Bizzi et al., 1991; d'Avella et al., 2006) and its variants have been widely employed to extract muscle synergy patterns from sEMG signals (Ting & McKay, 2007). Nevertheless, in practice, sEMG recordings are subject to numerous sources of distortion, including skin impedance variations, physiology complexity-based non-idealities and hardware noise. Noise-aware preprocessing is therefore crucial to improve factorization and ensure stable sEMG-based control regression. This study proposes a hybrid factorization framework that models noise and uncertainty, integrating the signal reconstruction and noise reduction capabilities of the Frisch scheme (Guidorzi et al., 2008) – an Errors-in-Variables method designed to reduce measurement noise effects – with the data-driven pattern

☆ This article is part of a Special issue entitled: 'IFAC WC 2026 - TC 8.2' published in IFAC Journal of Systems and Control.

* Corresponding author.
E-mail address: roberto.meattini@unibo.it (R. Meattini).

https://doi.org/10.1016/j.ifacsc.2026.100405

extraction strengths of NMF (Lin et al., 2018). This perspective differs from most recent strategies adopted to cope with sEMG noise, complexity and non-idealities. Indeed, a large portion of the state of the art face these challenges primarily through increasingly sophisticated pattern recognition and machine learning schemes, such as self-supervised regression models (Meattini et al., 2023), incremental and co-adaptive learning frameworks (Campbell et al., 2025; Schulz et al., 2025), progressive and incremental sparse NMF paradigms (Gigli et al., 2023), and transfer learning approaches aimed at domain adaptation (Wu et al., 2023). While these methods enhance robustness by refining or adapting the decoding stage, the present work adopts a complementary measurement-oriented viewpoint: before increasing model complexity, we explicitly estimate noise-consistent linear relations among sEMG channels within an Errors-in-Variables framework. In this way, the Frisch scheme is used to improve the statistical consistency of the input data prior to factorization, thereby strengthening the identifiability and stability of the subsequent NMF-based synergy extraction. The method was tested on five subjects performing four hand gestures and compared with standard NMF, sparse NMF with multiplicative update (NMF-MU), sparse NMF with alternating least squares (NMF-ALS), and the hybrid Frisch–NMF approach, with performance evaluated via RMSE against ground-truth control signals.

2. Methods

2.1. NMF and its variants

2.1.1. Muscle synergy concept

The estimation framework builds upon the neuromuscular principle of *muscle synergies*, according to which the central nervous system (CNS) coordinates motor tasks by activating groups of muscles through shared neural drives (Castellini & van der Smagt, 2013; d'Avella et al., 2006). Instead of controlling each muscle separately, the CNS activates a limited set of synergies that produce coordinated muscle patterns, enabling low-dimensional movement control, while each sEMG channel captures the volume-conducted activity of multiple motor units. The raw sEMG signal at a generic electrode s can be modeled as:

$$e_s(t) = \sum_{i=1}^{m} \sum_{j=1}^{N_i} g_{sij}(t) * f_{ij}(a_i(t)), \tag{1}$$

where "$*$" is the convolution operator, m is the number of muscles contributing to the signal, N_i is the number of MUs in muscle i, $f_{ij}(a_i(t))$ is the firing response of MU j modulated by related muscle activation $a_i(t)$, and $g_{sij}(t)$ is the impulse response describing the volume conduction between that MU and electrode s. In particular, the root mean square (RMS) value of the sEMG signal, computed over a short time window, is approximately proportional to underlying muscle activation (Jiang et al., 2009), and can be expressed as:

$$e_s^{\mathrm{RMS}}(t) = \sum_{i=1}^{m} e_{si}^{\mathrm{RMS}}(t) + \sum_{i=1}^{m} \sum_{h=1, h\neq i}^{m} \overline{e_{si}(t)\, e_{sh}(t)}, \tag{2}$$

where the first sum represents the contribution of each muscle i to the RMS signal, while the second accounts for cross-terms between muscles i and h due to volume conduction overlap and inter-channel crosstalk. The cross-product component $\overline{e_{si}(t)\, e_{sh}(t)}$ denotes the root mean value of the product $e_{si}(t)\, e_{sh}(t)$, computed over the same time window of the RMS value $e_s^{\mathrm{RMS}}(t)$. Assuming coordinated hand opening and closing driven by forearm flexion and extension, we can consider that the correlation of the terms $e_{si}(t)$ and $e_{sh}(t)$ in Eq. (2) is low, and that their cross-product terms are negligible, yielding the simplified linear model (Jiang et al., 2009):

$$e_s^{\mathrm{RMS}}(t) \approx \sum_{i=1}^{m} h_{si} a_i(t), \tag{3}$$

where h_{si} represents the average transmission gain between muscle i and electrode s. Assuming the collection of g channels, the sEMG vector can be expressed as:

$$E(t) = HA(t), \tag{4}$$

where $E(t) \in \mathbb{R}^g$ contains the RMS values from the g sEMG channels, $A(t) \in \mathbb{R}^{m\times 1}$ collects the muscle activations, and $H \in \mathbb{R}^{g\times m}$ is the activation-to-EMG mixture matrix. Now, assuming the hand has n degrees of freedom (DoF), actuated by k extensor and l flexor muscles, the vector of joint postures $\theta(t) = [\theta_1(t), \ldots, \theta_n(t)]^T$ can be modeled as a linear combination of *kinematic synergies* (Santello et al., 1998):

$$\theta(t) = P \begin{bmatrix} u_E(t) & u_F(t) \end{bmatrix}^T, \tag{5}$$

where $P \in \mathbb{R}^{n\times 2}$ is the *kinematic synergy matrix* and $u_E(t)$, $u_F(t)$ represent the neural drives associated with extensor and flexor control actions, respectively. The corresponding muscle activation vector $A(t) = [a_1(t), \ldots, a_{k+l}(t)]^T$ can be expressed as a linear mapping of the joint configuration:

$$A(t) = M\,\theta(t), \tag{6}$$

where $M \in \mathbb{R}^{(k+l)\times n}$ is the *muscular synergy matrix* describing how the activation of each muscle contributes to the joint postural synergies. Substituting (5) into (6) yields a compact expression that directly relates muscle activations to neural drives:

$$A(t) = MP \begin{bmatrix} u_E(t) & u_F(t) \end{bmatrix}^T = S_M U(t), \tag{7}$$

where $S_M = MP \in \mathbb{R}^{m\times 2}$ represents the *muscle synergy matrix* and $U(t) = [u_E(t)\ u_F(t)]^T$ is the vector of time-varying neural command signals associated with hand motion. Substituting this relation into Eq. (4) leads to the neuromuscular formulation:

$$E(t) = HS_M U(t) = WU(t), \tag{8}$$

where $W \in \mathbb{R}^{g\times 2}$ is the *drive-to-EMG mixture matrix*. It follows that an unsupervised linear factorization algorithm can be used to estimate $U(t)$ in Eq. (8) (Meattini et al., 2018). Specifically, we apply the NMF algorithm, as reported in the following.

2.1.2. NMF-based estimation of hand motion activation

To estimate the time-varying neural commands associated with each hand motion, the drive-to-EMG matrix $W = HS_M$ must first be identified from a training dataset acquired during specific gestures. Let $E_{\mathrm{train}} \in \mathbb{R}^{g\times N}$ denote the RMS sEMG samples collected over N time instants. According to the neuromuscular model, these data can be expressed as:

$$E_{\mathrm{train}} = WU_{\mathrm{train}}, \tag{9}$$

where $U_{\mathrm{train}} \in \mathbb{R}^{2\times N}$, according to Eq. (4), contains the neural drive components corresponding to flexion and extension. W and U_{train} are estimated via matrix factorization using NMF, which decomposes sEMG signals into physiologically interpretable components without requiring ground-truth labels (Meattini et al., 2018). In this study, NMF serves as the core factorization method used to estimate the underlying neural drives. Building on this, we will also explore variants of NMF, specifically sparse formulations with Multiplicative Update (MU) and Alternating Least Square (ALS) (Lin et al., 2018) — referred to as NMF-MU and NMF-ALS, respectively. Once W has been estimated, the neural

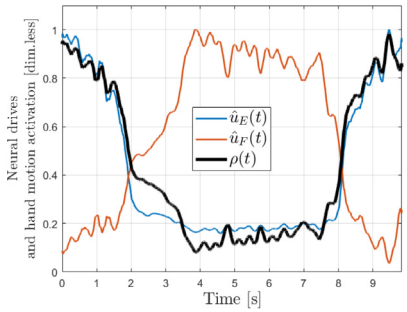

Fig. 1. Exemplary neural drives of the extensor ($\hat{u}_E(t)$) and flexor ($\hat{u}_F(t)$) muscle groups and the corresponding hand motion activation $\rho(t)$ for a power grasp motion.

drives for new (online) data $E_{\text{online}}(t)$ can be computed using its Moore–Penrose pseudo-inverse:

$$U_{\text{online}}(t) = \left[u_{E,\text{online}}(t)\; u_{F,\text{online}}(t)\right]^T = W^{\dagger} E_{\text{online}}(t).$$

Here, $u_{E,\text{online}}(t)$ and $u_{F,\text{online}}(t)$ represent the estimated neural drives associated with extensor and flexor activation, respectively. Because NMF-based decompositions are scale-invariant, the absolute magnitudes of these signals depend on the relative scaling between W and $U(t)$. Normalization factors are introduced from training data:

$$\gamma_E = \max(u_E(t)), \quad \gamma_F = \max(u_F(t)). \tag{10}$$

The normalized drives are then defined as:

$$\hat{u}_E(t) = u_E(t)/\gamma_E, \quad \hat{u}_F(t) = u_F(t)/\gamma_F, \tag{11}$$

ensuring that both vary within the range [0, 1]. Finally, the hand motion activation $\rho(t)$ is obtained as differential activation (Meattini et al., 2019):

$$\rho(t) = (\hat{u}_E(t) - \hat{u}_F(t) + 1)/2, \tag{12}$$

where $\rho(t) \in [0, 1]$. Physiologically, $\rho(t)$ represents the instantaneous normalized balance between extensor and flexor neural drives. A value of $\rho(t) = 0.5$ corresponds to equal activation of the two antagonist groups. Values greater than 0.5 indicate a predominance of extensor activity, whereas values lower than 0.5 indicate a predominance of flexor activity. The closer $\rho(t)$ is to 1 or 0, the more the hand is open or close, respectively. For clarity, Fig. 1 exemplarily shows the neural drives and the corresponding hand motion activation for a power grasp. Because $\rho(t)$ varies continuously, it provides an intuitive control variable for myoelectric or teleoperated robotic control.

2.2. The Frisch scheme

The Frisch Scheme (Guidorzi et al., 2008) is an estimation approach used to identify linear relationships when all variables are affected by additive noise. Let $x_1(t), x_2(t), \ldots, x_g(t)$ denote a set of g measured variables (signals). Since the measurements are affected by noise, no exact linear relation exists among the variables. The following assumptions are introduced:

(A1) Each variable can be expressed as the sum of a noise-free (exact) component and a noise term:

$$x_i(t) = \hat{x}_i(t) + \tilde{x}_i(t) \quad i = 1, \ldots, g \tag{13}$$

(A2) The noise-free variables are zero-mean ergodic processes, and linked by linear relations of the form

$$\alpha_1 \hat{x}_1(t) + \alpha_2 \hat{x}_2(t) + \cdots + \alpha_g \hat{x}_g(t) = 0 \tag{14}$$

(A3) The noise signals are zero-mean ergodic random processes whose variances are denoted by $\tilde{\sigma}_1^2, \ldots, \tilde{\sigma}_g^2$:

$$E[\tilde{x}_i(t)^2] = \tilde{\sigma}_i^2, \quad i = 1, \ldots, g \tag{15}$$

where $E[\cdot]$ denotes the expectation operator.

(A4) The noise variables are mutually independent:

$$E[\tilde{x}_i(t)\tilde{x}_j(t)] = 0, \quad \forall i, j, i \neq j \tag{16}$$

(A5) Noise variables are independent from noise-free ones:

$$E[\tilde{x}_i(t)\hat{x}_j(t)] = 0, \quad \forall i, j \tag{17}$$

Assume that N measurements are available for each variable and define the data matrix

$$X = \begin{bmatrix} x_1(1) & x_2(1) & \cdots & x_g(1) \\ x_1(2) & x_2(2) & \cdots & x_g(2) \\ \vdots & \vdots & & \vdots \\ x_1(N) & x_2(N) & \cdots & x_g(N) \end{bmatrix} \tag{18}$$

The (unknown) matrices of the noise-free data $\hat{X}$ and noise $\tilde{X}$ can be defined in a similar way. According to Assumption (A1) we have

$$X = \hat{X} + \tilde{X}. \tag{19}$$

Any linear relation among the noise-free variables can then be expressed as (see Assumption (A2))

$$\hat{X}\,A = 0, \quad \text{where } A = \begin{bmatrix} \alpha_1 & \alpha_2 & \ldots & \alpha_g \end{bmatrix}^T. \tag{20}$$

Consider the covariance matrix Σ of the measured data

$$\Sigma = \lim_{N\to\infty} \frac{X^T X}{N} \tag{21}$$

and, similarly, the (unknown) covariance matrices $\hat{\Sigma}$ and $\tilde{\Sigma}$ of the noise-free and noise sequences, respectively. From (19) and Assumptions (A5) it follows that

$$\Sigma = \hat{\Sigma} + \tilde{\Sigma}. \tag{22}$$

Moreover, according to Assumptions (A3) and (A4), the covariance matrix $\tilde{\Sigma}$ is diagonal

$$\tilde{\Sigma} = \text{diag}[\,\tilde{\sigma}_1^2\; \tilde{\sigma}_2^2\; \ldots\; \tilde{\sigma}_g^2\,]. \tag{23}$$

Any linear relation of the type (20) can be expressed as

$$\hat{\Sigma}\,A = 0. \tag{24}$$

Therefore, the matrix $\hat{\Sigma}$ is positive semidefinite with at least one eigenvalue equal to zero and the parameter vector A belongs to its null space. The Frisch scheme estimation problem can be stated as follows.

Frisch scheme. Given the covariance matrix of the noisy observations Σ, determine positive definite or positive semidefinite diagonal noise covariance matrices $\tilde{\Sigma}$ (see (23)) such that

$$\hat{\Sigma} = \Sigma - \tilde{\Sigma} \geq 0, \quad \det(\hat{\Sigma}) = 0. \tag{25}$$

Any basis of $\ker(\hat{\Sigma})$ describes a set of linear relations compatible with Assumptions (A1)–(A5). Let $P = (\,\tilde{\sigma}_1^2\; \tilde{\sigma}_2^2\; \ldots\; \tilde{\sigma}_g^2\,)$ be a point in the positive orthant $\mathbb{R}_+^g$ of $\mathbb{R}^g$ and let $\tilde{\Sigma}(P)$ denote the associated diagonal matrix $\text{diag}[\,\tilde{\sigma}_1^2\; \tilde{\sigma}_2^2\; \ldots\; \tilde{\sigma}_g^2\,]$. The Frisch scheme estimation problem consists of finding the set of points $P \in \mathbb{R}_+^g$ such that the matrix $\Sigma - \tilde{\Sigma}(P)$ satisfies condition (25). This set represents the locus of solutions of the Frisch scheme, and is described in the following theorem (Beghelli et al., 1990).

Theorem 1. *All the admissible solution in the noise space lie on a convex hypersurface $\mathcal{S}(\Sigma)$ contained in the positive orthant of $\mathbb{R}^g$. The concavity of $\mathcal{S}(\Sigma)$ faces the origin and its intersections with the coordinate axes are the points corresponding to the g least squares solutions (each obtained by assuming only one variable affected by noise).*

Every point $P \in \mathcal{S}(\Sigma)$ can be associated with a linear relation described by a matrix A, which can be obtained by computing any basis of the kernel of $\Sigma - \tilde{\Sigma}(P)$:

$$(\Sigma - \tilde{\Sigma}(P))A = 0, \quad \tilde{\Sigma}(P) = \text{diag}[\,\tilde{\sigma}_1^2\ \tilde{\sigma}_2^2\ \dots\ \tilde{\sigma}_g^2\,]. \tag{26}$$

A useful way to parameterize the hypersurface $\mathcal{S}(\Sigma)$ is provided by the following theorem (Guidorzi et al., 2008).

Theorem 2. *Let $\xi = (\xi_1, \dots, \xi_g)$ be a generic point in the positive orthant of $\mathbb{R}^g$ and r_ξ the straight line passing through the origin and ξ. The intersection $P = (\tilde{\sigma}_1^2, \dots, \tilde{\sigma}_g^2)$ between r_ξ and $\mathcal{S}(\Sigma)$ is given by*

$$P = \xi/\lambda_M, \tag{27}$$

where

$$\lambda_M = \max \text{eig}\left(\Sigma^{-1}\tilde{\Sigma}^\xi\right) \quad \textit{and} \quad \tilde{\Sigma}^\xi = \text{diag}\left[\,\xi_1,\ \dots,\ \xi_g\,\right].$$

This result is particularly useful for implementing the estimation scheme, as it allows to associate each admissible solutions with a straight line passing from the origin and lying in the positive orthant of $\mathbb{R}^g$.

Remark 1. In practice, the covariance matrix (21) is not available and the Frisch scheme is applied to its sample estimate

$$\Sigma^s = (X^T X)/N, \tag{28}$$

which can be computed from the measured signals. In this case, every point $P \in \mathcal{S}(\Sigma^s)$ yields a matrix $\Sigma^s - \tilde{\Sigma}(P)$ having only one eigenvalue equal to zero. Consequently, any basis of its null space is a vector A of the form (20).

2.3. A hybrid Frisch-NMF approach

The Frisch scheme is particularly suited to sEMG signals, which are inherently noisy due to measurement noise, cross-talk, and overlapping muscle activity. It is worth noting that, in this context, such nonidealities are treated as effective perturbations with respect to the adopted NMF-driven linear mixture model, rather than as intrinsically random physiological noise, so as to enable a consistent Errors-in-Variables formulation prior to NMF-based factorization. The proposed hybrid method combines the noise-reduction capability of the Frisch scheme with the unsupervised synergy extraction of NMF. Specifically, the Frisch method is first applied to obtain a denoised version $\hat{E}_{train}$ of the signal matrix E_{train} (9); then, non-negative matrix factorization is performed on $\hat{E}_{train}$. In this framework, the variables $x_1(t), x_2(t), \dots, x_g(t)$ to which the Frisch scheme is applied are the RMS of the sEMG signals collected from the g channels, so that $X = E_{train}^T$. In fact, according to (9), the ideal RMS data matrix should be rank-deficient, and the g RMS signals should be linked by linear relations. This is consistent with Eqs. (19), (20). According to Section 2.2, the sample covariance matrix Σ^s of the RMS data is computed (see (28)). It is then possible to define the Frisch locus $\mathcal{S}(\Sigma^s)$, which represents the set of admissible solutions in the noise space. Each point $P \in \mathcal{S}(\Sigma^s)$ can be associated with a linear relation among the "denoised" g RMS signals, obtained by computing a basis of the kernel of the singular matrix $\hat{\Sigma}(P) = \Sigma^s - \tilde{\Sigma}(P)$. At this stage, the goal is to select an optimal solution among the admissible ones; to this end, NMF is embedded within the Frisch scheme, as described below. From (19) and (21), the matrix $\hat{\Sigma}(P)$ can be interpreted as the sample covariance matrix of the (unknown) noise-free data matrix $\hat{X}(P)$:

$$\hat{\Sigma}(P) = (\hat{X}^T(P)\hat{X}(P))/N. \tag{29}$$

Consider the Singular Value Decomposition (SVD) (Golub & Van Loan, 2013) of $\hat{X}(P)$;

$$\hat{X}(P) = USV^T, \tag{30}$$

where U and V are orthogonal matrices, and S contains the singular values. Substituting (30) into (29) we get

$$\hat{\Sigma}(P) = (VS^TSV^T)/N = V\Lambda V^T, \tag{31}$$

which is the SVD of $\hat{\Sigma}(P)$, where $\Lambda = S^TS/N$ is the eigenvalue matrix and $S/\sqrt{N}$ is the square root of Λ: $\sqrt{\Lambda} = S/\sqrt{N}$. It is not possible to fully reconstruct $\hat{X}(P)$ from (31) since only V and S can be obtained from $\hat{\Sigma}(P)$. Therefore, the following approximation is adopted:

$$\hat{X}_{app}(P) = \sqrt{N}Z\sqrt{\Lambda}V^T, \tag{32}$$

where Z is a $g \times N$ random matrix whose entries follows a normal distribution $\mathcal{N}(0, 1)$. For sufficiently large N, the covariance matrix of Z approaches the identity, so transformation (32) preserves the data structure while ensuring statistical consistency. Once $\hat{X}_{app}(P)$ has been obtained, an NMF-based estimation of the hand motion activation is computed as described in Section 2.1. In particular, a NMF is first applied to the matrix $\hat{E}(P) = \hat{X}_{app}^T(P)$ to obtain the matrices $W(P)$ and $U(P)$

$$\hat{E}(P) = \hat{X}_{app}^T(P) \approx W(P)U(P). \tag{33}$$

where $U(P) \in \mathbb{R}^{2\times N}$ is the estimated neural drives matrix, that can be partitioned as follows (see (7), (8)):

$$U(P) = \left[U_E(P)\ \ U_F(P)\right]^T. \tag{34}$$

An estimate of the hand motion activations can then be obtained as:

$$\rho(P) = (\hat{U}_E(P) - \hat{U}_F(P) + 1)/2, \tag{35}$$

with $\hat{U}_E(P)$ and $\hat{U}_F(P)$ the normalized neural drives (see Eq. (11)). To select a single solution within the Frisch locus, the vector $\rho(P)$ is compared with the reference signal ρ_{ref} (the ground truth signal, see Section 3.2). The optimal solution minimizes the following loss function:

$$\|\rho(P) - \rho_{ref}\|. \tag{36}$$

Let $P_{opt} \in \mathcal{S}(\Sigma^s)$ be the point associated with the optimal solution. The corresponding matrix $\hat{E}(P_{opt}) = \hat{X}_{app}^T(P_{opt})$ represents the denoised version $\hat{E}_{train}$ of the matrix E_{train}. Therefore, the NMF of $\hat{E}(P_{opt})$ provides the drive-to-EMG mixture matrix $W(P_{opt})$ which is used for the online estimation of the hand motion activations (see Section 2.1). The proposed approach adopts a static (instantaneous) Frisch formulation, consistently with common multichannel sEMG modeling practice (see Table 1), in which volume conduction and cross-talk are captured through the linear relations among the latent noise-free variables (Eq. (14)), while Assumption A4 (Eq. (16)) constrains the additive noise terms to be mutually uncorrelated; under this interpretation, such non-idealities are embedded in the structural component of the model rather than in the noise term, and future work will extend the framework toward dynamic formulations to explicitly account for possible temporal effects induced by volume conduction. Note that using the reference signal ρ_{ref} in Eq. (36) makes the selection of P_{opt} supervised. However, the construction of the Frisch locus

Table 1
Comparison with recent sEMG decoding approaches.

Reference	Decoding	Main focus	Main result
Meattini et al. (2023)	NMF + Neural network	Self-supervised nonlinear regression	Multi-grasp decoding without explicit labeling
Campbell et al. (2025)	Incremental machine learning	Adaptation to non-stationarity	Taxonomy of methods and open challenges
Schulz et al. (2025)	Incremental sparse NMF	Unsupervised regression scalability	Up to 6 controllable muscle synergies
Wu et al. (2023)	Transfer learning	Cross-domain generalization	Reduced recalibration effort
This work	**Frisch + NMF**	**Noise-aware channel modeling**	**Noise-consistent modeling enhances unsupervised NMF regression**

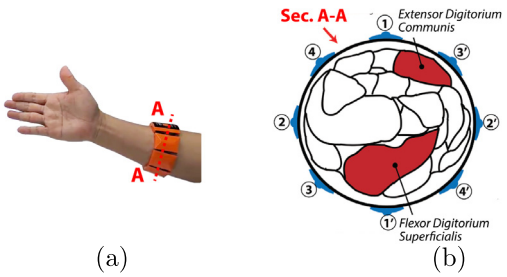

Fig. 2. Electrodes placement on the forearm. (a) sEMG armband. (b) Representation of forearm's section.

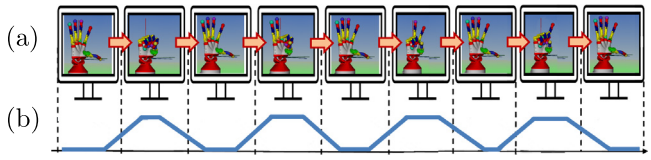

Fig. 3. (a) The motion of the simulated robotic hand. (b) Its hand motion activation used as ground truth.

$\mathcal{S}(\Sigma^s)$ and the generation of candidate denoised solutions remain fully unsupervised. In this work, we adopt this supervised selection to study whether a Frisch-denoised *s*EMG matrix exists that, once factorized via NMF, yields improved regression performance compared to NMF alone; investigating alternative selection criteria – including unsupervised options – is left to future work and is discussed in the Discussion section (Section 3.5).

3. Experimental evaluation

3.1. sEMG setup and preprocessing

Surface electromyographic (sEMG) signals were acquired using an OYMotion gForcePro armband (Fig. 2) with eight circumferential electrodes placed over the forearm to capture activity mainly from the *Flexor Digitorum Superficialis* and *Extensor Digitorum Communis* muscles, following standard guidelines (Perotto, 2011). Signals were preprocessed as in Meattini et al. (2018) using a 20 Hz high-pass Butterworth filter (4th order) and a 50 Hz notch filter to remove motion artifacts and power line interference (De Luca et al., 2010). Following filtering, each channel was converted to its RMS value using a 200 ms sliding window, remaining below typical human perceptual delay thresholds and thus not introducing appreciable lag. The RMS signal constitutes the main input for the subsequent experimentation, corresponding to the $E(t)$ formulation introduced in Section 2.1 (see Eq. (4)).

3.2. Experimental protocol and data description

sEMG signals were recorded from five healthy participants while performing four functional hand gestures representative of common grasping actions: *Power Grasp*, *Tripodal Grasp*, *Ulnar Grasp*, and *Index Point*. The four motions were selected to cover representative functional patterns with a limited set of commands suitable for proportional myoelectric control. Following the grasp taxonomy and the Virtual Finger (VF) rationale (Feix et al., 2015; Meattini et al., 2023), we considered three volar grasps characterized by different VF configurations (Power, Tripodal, Ulnar), so as to span distinct thumb–finger opposition strategies and flexor–extensor recruitment patterns. In addition, Index Point was included as a non-volar, extension-dominant functional gesture to evaluate the estimator also on a fine pointing action, complementing grasping with a commonly used command in prosthetic scenarios. Accordingly, our goal is not large-vocabulary gesture classification, but accurate continuous regression (local tracking) of a small set of functional motions enabling smooth and intuitive control. During each session, participants sat with the forearm supported while a simulated robotic hand (Fig. 3(a)) displayed slow, continuous opening and closing movements for four gestures. The hand performed six repetitions per gesture, always starting and ending open, and participants synchronized their motion in real time to minimize timing errors. sEMG signals were recorded simultaneously using the setup described in Section 3.1. In parallel, the time-varying closure level of the simulated robotic hand was recorded and stored as the reference signal representing the ground truth of the hand motion activation (Fig. 3(b)). Since subjects followed the displayed trajectory slowly and accurately, the reference signal was considered a reliable approximation of the true motion activation profile. The resulting sEMG recordings were then organized by gesture to form the dataset for subsequent analysis. As defined in Section 2.1, the preprocessed sEMG data were arranged into the matrix E_{train}, whose structure corresponds to that adopted in the proposed estimation framework (see Eq. (9) and Section 2.3). Fig. 4 illustrates an example of the acquisition sequence, showing the human hand gestures (top row), the corresponding sEMG signals, and the ground-truth.

3.3. Two-level nested (5×6)-fold cross-validation

To evaluate the proposed Frisch+NMF method against the other approaches, a two-level nested cross-validation (nCV) was performed for each subject to obtain an unbiased estimate of regression accuracy. The procedure used the sEMG datasets acquired as described previously (six repetitions of the four gestures: Power, Tripodal, Ulnar, and Index Point) and was structured as follows:

(i) **Outer loop:** one of the six repetitions was held out as test data, and the remaining five were used for training.
(ii) **Inner loop:** a 5-fold cross-validation was performed on the five training repetitions for hyperparameter tuning.
(iii) Each outer iteration produced five test evaluations, repeated over all six partitions for a total of $5 \times 6 = 30$ evaluations per subject.

The regression accuracy was quantified in terms of the Root Mean Square Error (RMSE) between the estimated and the ground-truth

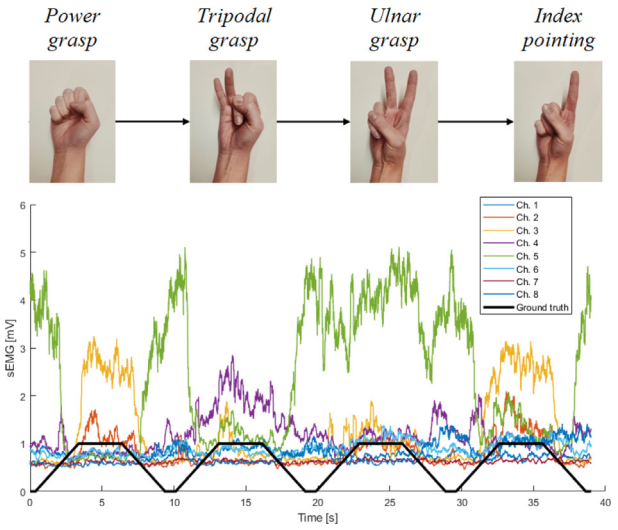

Fig. 4. Acquisition sequence with hand gestures, 8-channel sEMG signals, and ground truth (black signal).

hand motion activation $\rho(t)$, as defined in Eq. (12). RMSE values were averaged over the 30 folds for each subject and method to obtain a robust performance index. Evaluation included standard NMF, sparse NMF with multiplicative updates (NMF-MU), sparse NMF with alternating least squares (NMF-ALS), and the two hybrid variant (Frisch+NMF and Frisch+MU). Training and testing followed the estimation procedures described in Sections Section 2.1—2.3.

3.4. Global results

This section reports the experimental outcomes obtained by applying the proposed hybrid Frisch+NMF approach and the benchmark methods described in Section 2. Results are presented qualitatively through representative examples of the estimated hand motion activation $\rho(t)$, and quantitatively through the overall regression accuracy aggregated across subjects and gestures. Fig. 5 summarizes the qualitative results. In Fig. 5(a), each subplot (a.1–a.5) corresponds to one tested method (NMF, NMF-MU, NMF-ALS, Frisch+NMF, Frisch+MU) and reports the mean estimated $\rho(t)$ (solid blue) across subjects and gestures, together with the corresponding standard deviation (shaded area), compared against the ground truth (black dashed line). In Fig. 5(b), the ground truth trajectory (black dashed) is reported for each gesture (Power, Tripodal, Ulnar, Index Point), together with the corresponding estimates obtained by all methods, averaged across the five subjects. Fig. 5(c) complements the qualitative visualization by reporting boxplots of the Dynamic Time Warping (DTW) distance (Meattini et al., 2023) and smoothness metrics (with *smoothness* defined as the power of the first derivative of the hand motion activation), together with phase-specific RMSE values computed over the rise, steady, and fall segments of the movement. These quantitative indices provide a compact statistical summary of temporal alignment accuracy, trajectory regularity, and reconstruction performance across different movement phases. The quantitative comparison is reported in Fig. 6, which shows the distribution of RMSE values obtained through the nested cross-validation procedure described in Section 3.3, aggregated across all subjects and gestures and grouped by method. Overall, the proposed Frisch+NMF approach yielded the lowest RMSE with respect to NMF, NMF-MU, NMF-ALS and Frisch+MU. A repeated-measures ANOVA confirmed a significant main effect of the method on RMSE values, $F(4, 76) = 38.53$, $p < .01$. Mauchly's test indicated violation of sphericity ($W = 0.022$, $p < .01$), therefore the Greenhouse–Geisser correction was applied ($\varepsilon = 0.54$). Post-hoc pairwise comparisons with Bonferroni correction showed that Frisch+NMF differed significantly from all approaches (all $p < .01$), whereas no significant differences among NMF, NMF-ALS, and NMF-MU ($p > .05$).

3.5. Discussion

This subsection discusses the experimental findings with explicit reference to the qualitative and quantitative evidence reported in Figs. 5 and 6. From a qualitative standpoint, Fig. 5(a) shows that all methods are capable of reproducing the general temporal evolution of the reference signal. The figure provides an overall comparison of the average estimated hand motion activation $\rho(t)$ across subjects and gestures, together with the associated inter-subject variability. In this representation, the Frisch+NMF configuration exhibits a narrower shaded region compared to the other methods, suggesting reduced variability across subjects. Small amplitude mismatches are expected and not critical in the context of continuous myoelectric control, where the user can compensate in real time by modulating muscle effort to achieve the desired grasp or release level. This behavior is consistent with a human-in-the-loop proportional control paradigm, in which the user continuously receives real-time sensory feedback (e.g., visual feedback of the robotic hand motion) and can compensate small amplitude mismatches by modulating muscle effort within the closed control loop. Fig. 5(b) complements this view by reporting the gesture-specific trajectories averaged across subjects. This panel allows a qualitative comparison of how the different methods follow the reference signal for each gesture. While the curves provide insight into the overall temporal behavior of the estimators, they do not by themselves allow precise conclusions regarding relative performance; rather, they offer a descriptive visualization of the reconstruction trends across configurations. A further observation concerns the hybrid configuration combining the Frisch scheme with sparse NMF based on the Alternating Least Squares update rule (Frisch+ALS). This variant failed to converge reliably and was therefore excluded from the reported results. The lack of convergence can be attributed to the approximated nature of the Frisch-denoised matrix $\hat{E}$, which represents a reduced version of the original dataset. When combined with sparsity constraints, this reduced representation may not retain sufficient information for the ALS optimization to converge, resulting in unstable decompositions. For this reason, the Frisch+ALS configuration is not included in Figs. 5 and 6. The indicators shown in Fig. 5(c) further support the qualitative observations by providing distributional evidence of temporal alignment (DTW), signal regularity (smoothness), and phase-dependent reconstruction accuracy. In particular, the phase-specific analysis allows a more detailed assessment of method behavior during the dynamic (rise and fall) and steady portions of the gesture, offering additional insight beyond the visual inspection of the averaged trajectories. The quantitative analysis reported in Fig. 6 provides a systematic assessment of performance differences, showing that the RMSE distributions aggregated across subjects and gestures exhibit a systematic reduction for the Frisch+NMF method. The statistical analysis presented in the previous subsection confirms that this reduction is significant with respect to all other tested approaches, supporting with statistical evidence the improvement associated with Frisch+NMF. Overall, the combined interpretation of Figs. 5 and 6, together with the statistical results reported in the preceding subsection, indicates that incorporating a noise-aware denoising stage within the synergy-based regression framework leads to improved reconstruction accuracy.

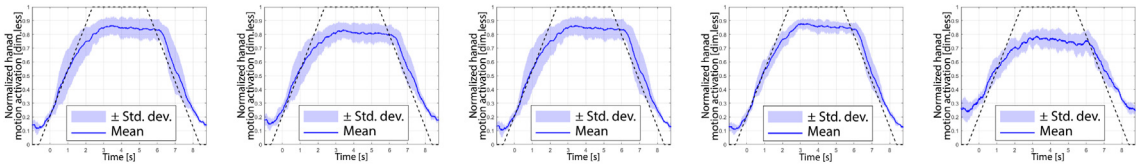

(a.1) NMF (a.2) NMF-MU (a.3) NMF-ALS (a.4) Frisch+NMF (a.5) Frisch+MU

(a) Mean estimated hand motion activation $\rho(t)$ vs. ground truth for each method (a.1–a.5).

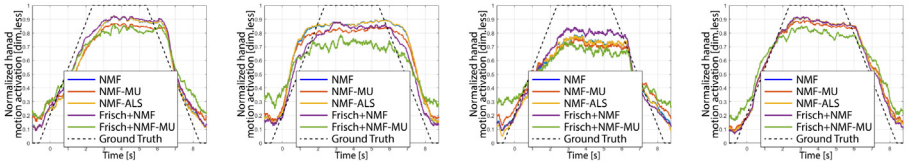

(b.1) Power grasp (b.2) Tripodal grasp (b.3) Ulnar grasp (b.4) Index pointing

(b) Estimated hand motion activation $\rho(t)$ for each gesture (b.1–b.4) across different methods.

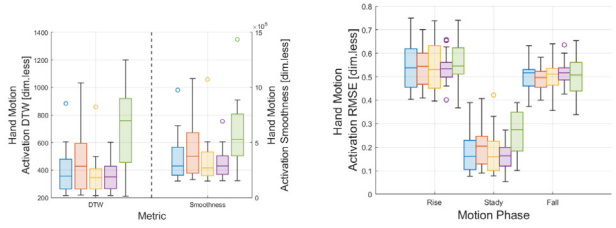

(c) DTW and smoothness (left), and phase-specific performance (right) metrics across methods.

Fig. 5. (a) Mean estimated hand motion activation $\rho(t)$ (solid blue) compared with ground truth (black dashed line) for all subjects and gestures, for each method (a.1–a.5). (b) Estimated hand motion activation $\rho(t)$ for each gesture (b.1–b.4), showing the comparison among all methods (colored lines) and the ground truth (black dashed line). (c) DTW, smoothness, and phase-specific performance indices.

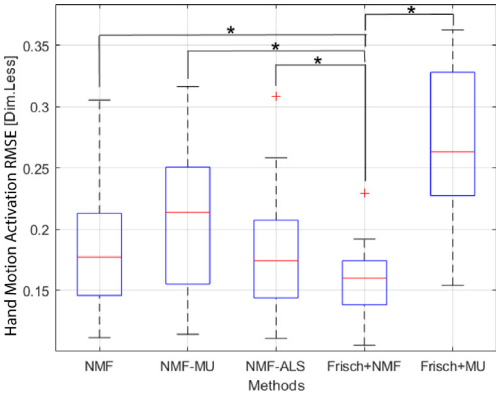

Fig. 6. RMSE across subjects and gestures by method; "∗" marks differences from Frisch+NMF ($p < .01$).

Eventually, we acknowledge that the number of enrolled subjects was limited, which may reduce the generalizability of the present findings. In inferential statistics, the sample size directly influences both the precision of the estimated effects and the probability of correctly detecting a true effect (i.e. the *statistical power*), whereas the significance level $\alpha = 0.05$ represents the conventional threshold used to control the probability of false-positive conclusions. Although a large effect size was observed in the present sample, effect estimates derived from small cohorts may be less stable and potentially inflated with respect to the underlying population effect. For this reason, future investigations should be designed under more conservative assumptions, namely considering medium-to-large effect sizes and targeting a statistical power of 0.80–0.90, corresponding to an 80–90% probability of detecting a true effect while maintaining a 5% false-positive rate. Under these conditions, a repeated-measures design with five experimental conditions would require approximately 20 to 30 subjects to ensure more reliable parameter estimation and stronger external validity. Future work will therefore aim at replicating the present analysis on larger cohorts in order to further assess the robustness and generalizability of the proposed approach. We also acknowledge that the present experiments were conducted under controlled forearm orientation. In practical prosthetic use, variations in limb posture may induce the well-known *limb position effect* (Campbell et al., 2025), altering sEMG distributions and potentially affecting regression accuracy. This issue is common to sEMG-based decoding systems in general and is typically addressed through incremental or adaptive retraining strategies incorporating data from multiple limb configurations. From a broader perspective, the proposed hybrid formulation can be positioned within the recent evolution of sEMG-based control strategies, as summarized in Table 1. While most contemporary approaches address signal non-idealities by increasing the complexity or adaptivity of the decoding stage (e.g., self-supervised regression, incremental learning, or transfer learning), the present work adopts a complementary measurement-oriented viewpoint. Instead of refining the decoder alone, we explicitly model noise-consistent linear relations among sEMG channels prior to factorization, thereby improving the statistical consistency of the data entering the NMF stage. This distinction highlights that enhanced regression performance can be achieved not only through more sophisticated learning schemes, but also through principled noise-aware modeling of the EMG measurements.

4. Conclusion

A hybrid method combining the Frisch noise-reduction scheme with Non-Negative Matrix Factorization was proposed for continuous hand motion estimation from sEMG signals. The approach improved robustness and accuracy over standard NMF-based techniques by explicitly accounting for measurement noise, cross-talk and non-idealities. Experimental results on five subjects confirmed that the Frisch+NMF approach achieved the lowest reconstruction error, highlighting its potential for more stable and interpretable myoelectric control of artificial hands.

CRediT authorship contribution statement

Roberto Meattini: Writing – review & editing, Writing – original draft, Supervision, Software, Methodology, Investigation, Data curation, Conceptualization. **Francesco Monti:** Writing – review & editing, Writing – original draft, Software, Methodology, Investigation, Data curation, Conceptualization. **Luca Bertozzi:** Writing – review & editing, Writing – original draft, Software, Methodology, Investigation, Data curation, Conceptualization. **Hamid Sohrabi:** Writing – review & editing, Writing – original draft, Software, Methodology, Investigation, Data curation, Conceptualization. **Davide Bargellini:** Writing – review & editing, Writing – original draft, Software, Methodology, Investigation, Data curation. **Roberto Diversi:** Writing – review & editing, Writing – original draft, Supervision, Software, Methodology, Investigation, Data curation, Conceptualization.

Declaration of competing interest

The authors declare the following financial interests/personal relationships which may be considered as potential competing interests: Roberto Meattini reports financial support was provided by European Commission. If there are other authors, they declare that they have no known competing financial interests or personal relationships that could have appeared to influence the work reported in this paper.

Acknowledgments

This work was supported in part by European Commission's Horizon Europe Framework Programme with the project IntelliMan under Grant 10107013.

References

Beghelli, S., Guidorzi, R., & Soverini, U. (1990). The frisch scheme in dynamic system identification. *Automatica*, *26*(1), 171–176.

Bizzi, E., Mussa-Ivaldi, F. A., & Giszter, S. (1991). Computations underlying the execution of movement: a biological perspective. *Science*, *253*(5017), 287–291.

Campbell, E., Egle, F., Oßwald, M., Côté-Allard, U., Pilarski, P. M., Boccardo, N., Meattini, R., Vujaklija, I., Hargrove, L., Canepa, M., et al. (2025). (Un) supervised (co) adaptation via incremental learning for myoelectric control: Motivation, review, and future directions. *IEEE Transactions on Neural Systems and Rehabilitation Engineering*.

Castellini, C., & van der Smagt, P. (2013). Evidence of muscle synergies during human grasping. *Biological Cybernetics*, *107*(2), 233–245.

d'Avella, A., Portone, A., Fernandez, L., & Lacquaniti, F. (2006). Control of fast-reaching movements by muscle synergy combinations. *Journal of Neuroscience*, *26*(30), 7791–7810.

De Luca, C. J., Gilmore, L. D., Kuznetsov, M., & Roy, S. H. (2010). Filtering the surface EMG signal: Movement artifact and baseline noise contamination. *Journal of Biomechanics*, *43*(8), 1573–1579.

Feix, T., Romero, J., Schmiedmayer, H.-B., Dollar, A. M., & Kragic, D. (2015). The grasp taxonomy of human grasp types. *IEEE Transactions on Human-Machine Systems*, *46*(1), 66–77.

Gigli, A., Gijsberts, A., Nowak, M., Vujaklija, I., & Castellini, C. (2023). Progressive unsupervised control of myoelectric upper limbs. *Journal of Neural Engineering*, *20*(6), Article 066016.

Golub, G. H., & Van Loan, C. F. (2013). *Matrix computations*. JHU Press.

Guidorzi, R., Diversi, R., & Soverini, U. (2008). The frisch scheme in algebraic and dynamic identification problems. *Kybernetika*, *44*(5), 585–616.

Jiang, N., Englehart, K. B., & Parker, P. A. (2008). Extracting simultaneous and proportional neural control information for multiple-DOF prostheses from the surface electromyographic signal. *IEEE Transactions on Biomedical Engineering*, *56*(4), 1070–1080.

Jiang, N., Parker, P. A., & Englehart, K. B. (2009). Spectrum of the nonstationary electromyographic signal modelled with integral pulse frequency modulation and its application to estimating neural drive information. *Journal of Electromyography and Kinesiology*, *19*(4), e267–e279.

Lin, C., Wang, B., Jiang, N., & Farina, D. (2018). Robust extraction of basis functions for simultaneous and proportional myoelectric control via sparse non-negative matrix factorization. *Journal of Neural Engineering*, *15*(2), Article 026017.

Meattini, R., Benatti, S., Scarcia, U., De Gregorio, D., Benini, L., & Melchiorri, C. (2018). An sEMG-based human–robot interface for robotic hands using machine learning and synergies. *IEEE Transactions on Components, Packaging and Manufacturing Technology*, *8*(7), 1149–1158. http://dx.doi.org/10.1109/TCPMT.2018.2799987.

Meattini, R., Caporali, A., Bernardini, A., Palli, G., & Melchiorri, C. (2023). Self-supervised regression of sEMG signals combining non-negative matrix factorization with deep neural networks for robot hand multiple grasping motion control. *IEEE Robotics and Automation Letters*, *8*(12), 8533–8540.

Meattini, R., De Gregorio, D., Palli, G., & Melchiorri, C. (2019). Design and evaluation of a factorization-based grasp myoelectric control founded on synergies. In *2019 12th international workshop on robot motion and control* (pp. 252–257). IEEE.

Perotto, A. O. (2011). *Anatomical guide for the electromyographer: the limbs and trunk*. Charles C Thomas Publisher.

Rehbaum, H., Jiang, N., Paredes, L., Amsuess, S., Graimann, B., & Farina, D. (2012). Real time simultaneous and proportional control of multiple degrees of freedom from surface EMG: preliminary results on subjects with limb deficiency. In *2012 annual international conference of the IEEE engineering in medicine and biology society* (pp. 1346–1349). IEEE.

Santello, M., Bianchi, M., Gabiccini, M., Ricciardi, E., Salvietti, G., Prattichizzo, D., Ernst, M., Moscatelli, A., Jörntell, H., Kappers, A. M., et al. (2016). Hand synergies: Integration of robotics and neuroscience for understanding the control of biological and artificial hands. *Physics of Life Reviews*, *17*, 1–23.

Santello, M., Flanders, M., & Soechting, J. F. (1998). Postural hand synergies for tool use. *Journal of Neuroscience*, *18*(23), 10105–10115.

Schulz, A., Egle, F., Osswald, M., Del Vecchio, A., & Castellini, C. (2025). Towards unsupervised incremental and proportional myocontrol based on higher-density surface electromyography. In *2025 international conference on rehabilitation robotics* (pp. 1106–1111). IEEE.

Ting, L. H., & McKay, J. L. (2007). Neuromechanics of muscle synergies for posture and movement. *Current Opinion in Neurobiology*, *17*(6), 622–628.

Wu, D., Yang, J., & Sawan, M. (2023). Transfer learning on electromyography (EMG) tasks: Approaches and beyond. *IEEE Transactions on Neural Systems and Rehabilitation Engineering*, *31*, 3015–3034.

Young, A. J., Smith, L. H., Rouse, E. J., & Hargrove, L. J. (2012). Classification of simultaneous movements using surface EMG pattern recognition. *IEEE Transactions on Biomedical Engineering*, *60*(5), 1250–1258.